

Original Article

Retinal Fundus Image-Based Analysis of Diabetic Retinopathy Detection and Classification Model Using Improved Dung Beetle Optimization with Deep Transfer Learning Techniques

A. Kokila^{1,*}, R. Shankar², S. Duraisamy³

^{1,2,3}Department of Computer Science, Chikkanna Government Arts College, Vivekananda Nagar, Konganagiri, Tiruppur, Tamil Nadu, India.

*Corresponding Author : 195kokila@gmail.com

Received: 13 April 2025

Revised: 14 May 2025

Accepted: 15 June 2025

Published: 27 June 2025

Abstract - Diabetic Retinopathy (DR) is a microvascular difficulty of diabetes and a primary reason for vision loss in the developed or developing world. DR typically starts as initial microvascular modifications in the retinal blood vessels. For DR's recognition and development study, colour fundus images are the best approach for non-invasive eye fundus imaging. Recent automated techniques for DR grading combine the recognition of each symptom. In recent years, Deep Learning (DL) models were presented to automatically measure DR, a predominant vision-impairing disorder, helping ophthalmologists express individualized treatment approaches for patients. In this study, a Retinal Fundus Image-Based Analysis of Diabetic Retinopathy Detection Using Improved Dung Beetle Optimization and Deep Transfer Learning Techniques (RFIADRD-IDBODTLT) technique is proposed. The proposed RFIADRD-IDBODTLT technique relies on the advanced and automatic model for DR classification and grading on fundus images. Initially, image pre-processing is performed using the Sobel Filter (SF) model to remove noise in an input image dataset. Furthermore, the CapsNet model is employed for feature extraction. The Bidirectional Long Short-Term Memory (BiLSTM) model is utilized to classify DR. Finally, the hyperparameter selection of the BiLSTM model is performed by implementing the Improved Dung Beetle Optimization (IDBO) model. Experimentation is performed to validate the RFIADRD-IDBODTLT approach under the DR detection dataset. The performance validation of the RFIADRD-IDBODTLT approach demonstrated a superior accuracy value of 95.30% over existing models.

Keywords - Diabetic Retinopathy, Retinal Fundus Image, Improved Dung Beetle Optimization, Deep Learning, Image Pre-Processing.

1. Introduction

Globally, DR is the main reason for vision loss. There is sufficient technical evidence that vision loss might be prevented through adequate treatment and early detection [1]. Nevertheless, this situation is asymptomatic and usually is undetectable until a progressive vision-threatening phase. Thus, regular DR screening programs focused on surveillance, primary analysis, and timely DR treatments are needed [2]. In such initiatives, severity grading and DR detection are accomplished by trained experts over visual examination of fundus images [3]. The primary concern is practice; the physical examination of these images includes a workload owing to the increased dominance of DR and the inadequate source of personnel and technology [4]. In such a case, the Computer-Aided Diagnosis (CAD) method might significantly help ophthalmologists study fundus images. With this method, DR analysis might be enhanced in terms

of speed, confidence, and accuracy while decreasing health costs and the workload of specialists [5]. Precise classification and Prompt detection of DR are vital for early treatment and intervention that can significantly reduce the risk of severe visual loss [6].

Fundus images are generally utilized for fundus observation, as they display the interior retina framework. Studying fundus imageries makes it possible to find lesions and perform comprehensive, thorough diagnosis and screening [7]. The study of fundus images is focused on the retinal lesion's recognition, and the DR might be classified depending on the kind and amount of identified abrasions. The grading DR task has recently gained notice from investigators in ophthalmology Machine Learning (ML), Artificial Intelligence (AI), and DL areas. DR grading is mainly deliberated as a classification task [8]. Scientists have



advanced rule-based methods to categorize the seriousness of DR. These models frequently comprise the utilization of a Convolutional Neural Network (CNN) to examine and subdivision key aspects in retinal images, like the retinal vasculature, retinopathy signals, and optic disc [9]. The aim is to automate the grading procedure, allowing early intervention and detection essential for protecting vision in patients with diabetes. The latest progression in Computer Vision (CV) and DL has determined the possibility of tackling these challenges [10].

In this study, a Retinal Fundus Image-Based Analysis of Diabetic Retinopathy Detection Using Improved Dung Beetle Optimization and Deep Transfer Learning Techniques (RFIADRD-IDBODTLT) technique is proposed. The proposed RFIADRD-IDBODTLT technique relies on the advanced and automatic model for DR classification and grading on fundus images. Initially, image pre-processing is performed using the Sobel Filter (SF) model to remove noise in an input image dataset. Furthermore, the CapsNet model is employed for feature extraction. The Bidirectional Long Short-Term Memory (BiLSTM) model is utilized to classify DR. Finally, the hyperparameter selection of the BiLSTM model is performed by implementing the Improved Dung Beetle Optimization (IDBO) model. Experimentation is performed to validate the RFIADRD-IDBODTLT approach under the DR detection dataset.

- The RFIADRD-IDBODTLT model employs SF for effective image pre-processing, improving edge features crucial for detecting retinal abnormalities. This step enhances the quality of input images by highlighting lesion boundaries. It significantly improves the accuracy and consistency of succeeding feature extraction and classification.
- The RFIADRD-IDBODTLT approach utilizes CapsNet for robust and spatially-aware feature extraction from pre-processed fundus images, preserving the hierarchical relationships between features. This allows the model to capture fine-grained patterns and discrepancies in retinal structures. It improves the capability of the method to distinguish between diverse stages of DR with improved precision.
- The RFIADRD-IDBODTLT method implements the BiLSTM network to capture sequential dependencies in the extracted features for accurate DR classification. It processes data in both forward and backward directions, enabling an overall understanding of complex patterns. This strengthens the model's temporal learning capability, resulting in more reliable classification outputs.
- The RFIADRD-IDBODTLT methodology utilizes the IDBO model for tuning the model parameters, ensuring higher results in DR detection. By effectively balancing exploration and exploitation, IDBO improves convergence speed and solution quality. This

optimization significantly enhances classification accuracy and model robustness across diverse datasets.

- The RFIADRD-IDBODTLT method integrates SF, CapsNet, BiLSTM, and IDBO models and is introduced for DR detection from fundus images. This incorporation uniquely utilizes edge enhancement, spatial hierarchy, temporal learning, and intelligent parameter tuning. The novelty is in the synergistic use of these components to address challenges in feature preservation and classification accuracy. It results in an efficient, lightweight, and highly accurate diagnostic model.

2. Related Works

Ravala and Rajini [11] developed an innovative approach to identify DR over the seriousness scaling by monitoring the irregularities over ensemble models. RSHWE is used to keep brightness, and segmented ensemble models recognize ROI. A feature map is formed by applying Gabor and Gaussian filter coefficients and GLCM aspects, and it is utilized to RFC and categorize the diseased images. In [12], an innovative screening of the DR model utilizing an asymmetrical DL feature is presented. Then, U-Net segments and a CNN with the SVM method are utilized to classify DR lesions. Sivapriya et al. [13] proposed an innovative approach for spontaneously partitioning the capillaries and classifying DR by applying fundus images. The U-Net is utilized as the basic structure to improve the segmentation technique. ResEAD2Net was developed in this study, whereas the upsampling and downsampling layer counts decreased. Palaniswamy and Vellingiri [14] projected an innovative IoT and DL-assisted diagnosis of the DR technique (IoTDL-DRD) method. Subsequently, pre-processing is performed to extract sound and enhance contrast. Furthermore, a based classifier and DenseNet-based feature extraction are utilized for effectual DR detection. The LSTM parameter optimization approach is also achieved using the Honey Bee Optimization (HBO) technique.

Arora et al. [15] proposed a novel DL structure for DR detection. The presented structure employs the EfficientNet-B0 structure to categorize DR severity stages from retinal images. By leveraging progressive models in ML and CV, the presented technique focused on delivering dependable and precise DR identifications. This structure takes support from the EfficientNet ML models and utilizes innovative CNN layering models. Wan et al. [16] introduced a WSN structure, and this structure creates a Transformer and CNN backbone in a parallel method. A New lightweight DL technique called *MobileViT – Plus* is presented to employ the HybridLG Transformer backbone model, and training approaches are influenced by an ensemble learning method intended to enhance the method's generalizability. In [17], the primary goal is to automate the DR classification process into multiple phases utilizing CNN techniques.

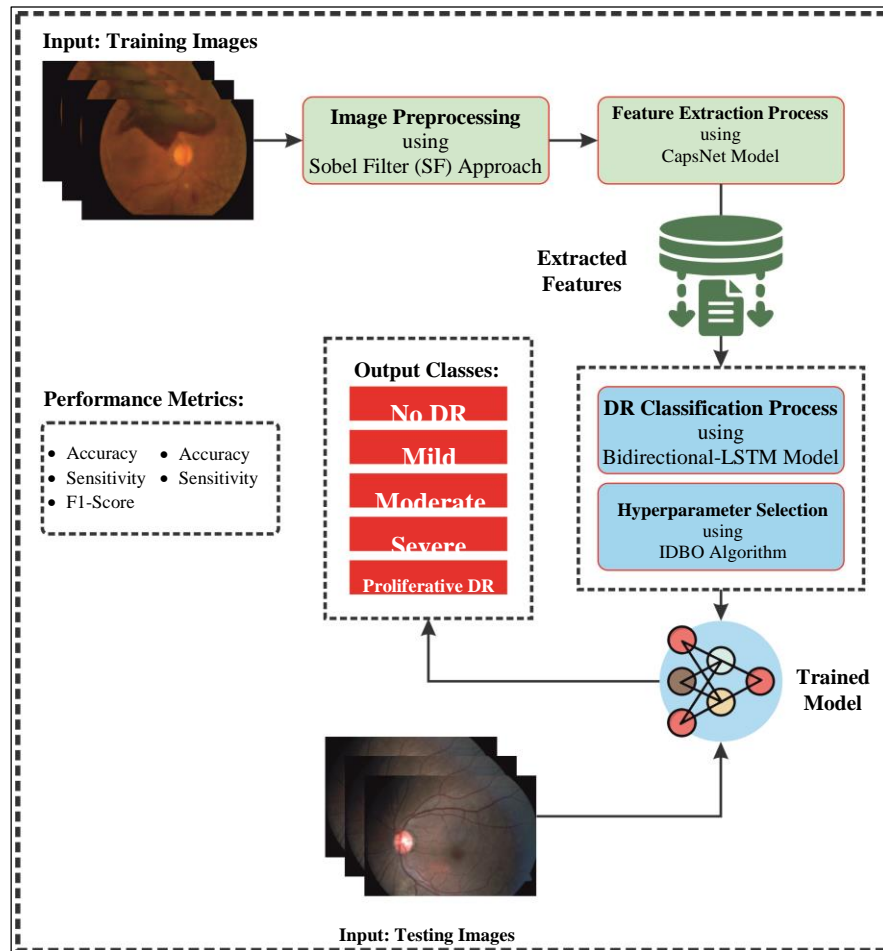


Fig. 1 Overall flow of the RFIADRD-IDBODTLT technique

This model implemented 15 pre-trained methods with the newly presented DR Network (DRNet13) technique. This paper focused on discriminating the most effective model. This approach pre-processed the image utilizing a Gamma correction for image enhancement and a median filter for noise reduction. Al-Kahtani et al. [18] developed a Discrete Migratory Bird Optimizer with Transfer Learning-based Multi-Retinal Disease Detection (DMBOTL-MRDD) method by integrating Wiener Filtering (WF) for noise removal, ShuffleNetv2 for feature extraction with optimized hyperparameters using Discrete Migratory Bird Optimizer (DMBO), and a Multi-Layer Autoencoder (MLA) model for disease classification.

Raza et al. [19] introduced a robust Transfer Learning (TL) model integrating MobileNet with constriction Factor-based Particle Swarm Optimization (MOB-CFPSO) for accurate classification. Mutawa et al. [20] presented Multi-Scale Discriminative Robust Local Binary Pattern (MS-DRLBP) features and a hybrid CNN-Radial Basis Function (CNN-RBF) classifier improved by stochastic modeling and advanced image preprocessing. Natarajan et al. [21] utilized DL and TL techniques to accurately diagnose and classify

multiple diseases using medical imaging datasets. Sushith et al. [22] proposed a hybrid CNN-Recurrent Neural Network (CNN-RNN) method with an Attention Mechanism (AM) for DR detection by utilizing both spatial and temporal features from retinal fundus images. Kamal et al. [23] proposed a novel DR detection method using synthetic data generation, K-Means clustering-Based Binary Grey Wolf Optimizer (BGWO), and fully convolutional encoder-decoder networks for accurate classification and feature extraction. Dixit and Jha [24] presented a TL-based DR classification method using EfficientNetB3 with Squeeze and Excitation (SE) blocks for accurate multiclass detection. Prabhakar et al. [25] proposed an optimization-based DL methodology by using U-Net segmentation and the Deep Q Network (DQN) model for accurate DR detection.

Despite significant progress in DR detection, various existing models still encounter threats such as limited generalizability across heterogeneous datasets, high computational complexity, and dependency on extensive annotated data. Several approaches lack robustness in multi-stage classification or do not fully employ spatial-temporal features. A key research gap is in integrating lightweight yet

effective DL methods with advanced optimization techniques to improve accuracy, mitigate error rates, and ensure adaptability across diverse imaging modalities.

3. The Proposed Model

This study presents an RFIADRD-IDBODTLT method. The introduced approach relies on an advanced and automatic model for DR classification and grading on fundus images. The technique comprises SF-based image pre-processing, CapsNet-based extraction, BiLSTM-based DR classification, and IDBO-based tuning processes defined in Figure 1.

3.1. Image Pre-Processing

The SF technique utilizes the RFIADRD-IDBODTLT model for performing the image pre-processing process [26]. The SF model is an extensively applied edge detection approach in image processing, mainly for underlining regions of interest in medical imaging, like fundus images, for the detection of DR. It works by computing the gradient magnitude in either horizontal or vertical directions, successfully recognizing edges while pixel intensity modifications quickly. Regarding DR detection, the SF helps separate blood vessels, micro-aneurysms, and other pathological features by improving their visibility. This pre-processing phase is essential for enhancing the precision of the following classification and grading methods. Its efficiency and simplicity make it a helpful device in CAD techniques for DR.

3.2. CapsNet-Based Feature Extraction

The RFIADRD-IDBODTLT technique performs feature extraction using the CapsNet technique [27]. A neural network structure named CapsNet was produced to get about a few of the disadvantages of traditional CNNs, most significantly its inability to characterize hierarchic spatial relations amongst characteristics. Scalar activations, the basis of extraction of the feature in CNNs, recognize the presence of the characteristic and then unclear significant particulars for its spatial features. In contrast, capsules-groups of neurons that give vectors, are presented by CapsNet. These vectors definite the object's orientation and position, pose other instantiate features and only show the object's presence (like an object portion). These vectors are impacted squashing functions that preserve orientation but compress length to values amongst (0, 1) to promise, which outputs of the capsule are constrained between (0, 1). CapsNet is very beneficial for medical imaging study since it encodes the existence and spatial properties, like size and orientation of features, so it becomes insensitive to scaling or rotation variations. They might design part-whole relationships fairly efficiently and take anatomic hierarchies critical in healthcare data.

The convolution layer's primary critical capsule layer feature mapping is systematized into capsules during this Primary Capsule Layer. For instance, numerous feature

mappings can provide capsules, all contributing to the vectors' size. The individual neuron of the CNN cannot encode as much data about an identified characteristic as the capsule vectors that help the networks understand the relations amongst entity portions. This approach ensures that low-level capsules, which detect basic features, activate high-level capsules for advanced features only when there is a stronger consensus. All low-level capsules use the transformation matrix to determine relations among them and predict high-level capsules. The outcome is prediction vectors. This coefficient is changed with dynamism by the iteration process, which evaluates the agreements amongst capsules and the function of softmax. The routing coefficient is higher, supporting the connection amongst these capsules after a prediction equals the high-level capsule output.

This network is tailored for the marginal loss function for the image classification task. These losses are dissimilar from conventional CNNs that use cross-entropy or softmax loss models. This margin loss was presented by lower and higher conditions to guarantee that the accurate class capsule gave longer vectors, whereas the in-error class capsule gave shorter ones. It is helped in taking fine-grained possessions by applying loss of reconstruction. By reconstructing the input images utilizing the output of the capsule, the model intends to reduce the Mean Squared Error (MSE) and amount of dissimilarity between the rebuilt and original imageries. This results in the inspiration of intricate, discriminate characteristics within the capsules. Finally, a few of the major problems by CNNs are solved by CapsNets. Therefore, it can process variations, namely rotations and perspective moves, additionally successfully. Since it might be learning more informational feature representations and is stronger to refine transform than CNNs. Figure 2 depicts the architecture of CapsNet.

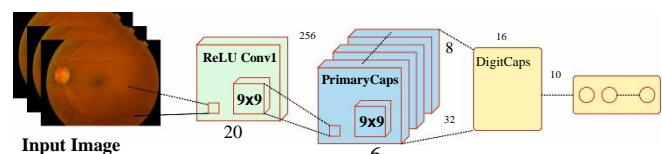


Fig. 2 Structure of CapsNet model

3.3. BiLSTM-based DR Classification

The RFIADRD-IDBODTLT method utilizes the BiLSTM model to classify the DR [28]. Training DL techniques, namely Bi-LSTM or LSTM models, is normal. Nevertheless, this is less effective and time-consuming in discovering the top structures. This is mainly true after the data shows complex sequential patterns and temporal dependencies. Whereas LSTM can take previous dependences, it might not implement additionally in tasks needing upcoming information consideration. The Bi-LSTM model combines three gates- the forget (f_t), the output (o_t), and the input (i_t)-to control the flow of data successfully. To successfully process the removal of a larger amount of

information at the final instant, they could apply the forget gate, signified as f_t :

$$f_t = \sigma(W_f[h_{t-1}, x_t] + b_f) \quad (1)$$

The input gate or i_t Normalizes the amount of data that needs direct storage.

$$f_t = \sigma(W_i[h_{t-1}, x_t] + b_i) \quad (2)$$

The present neuron counts require being transferred to the following neuron controlled by the output gate, o_t .

$$o_t = \sigma(W_o[h_{t-1}, x_t] + b_o) \quad (3)$$

$$C_t = \tanh(W_c[h_{t-1}, x_t] + b_c) \quad (4)$$

$$C_t = (f_t * C_{t-1}) + (i_t * C_{t-1}) \quad (5)$$

$$h_t = (o_t * \tanh(C_t)) \quad (6)$$

The weighted matrix is represented as W , h_{t-1} characterizes the preceding system output, h_t characterizes the recent result of the system and C_t Characterizes the inner variables of the LSTM model, which keeps information equal to the present moment. Simultaneously, the candidate state is represented in its letter. \tilde{C}_t . The input is characterized by x_t , the biased term was symbolized as $b_{(\cdot)}$. The logistical task was described by $\sigma_{(\cdot)}$. And the function of the activation is $\tanh(\cdot)$.

$$\sigma(x) = (1 + \exp(-x))^{-1} \quad (7)$$

$$\tanh(x) = 2\sigma(2x) - 1 \quad (8)$$

At t time, the cell of LSTM obtains three inputs: the preceding outcome of the time. (h_{t-1}), the present cell state (C_{t-1}), and the network input value (x_t). The cell may carry out its tasks by using three inputs. At some point, the cell gives dual outputs: the *output's* h_t value and the cell's present state represented as C_t .

3.4. IDBO-based Hyperparameter Tuning

The RFIADRD-IDBODTLT model performs a hyperparameter tuning process using the IDBO approach [29]. The DB's natural behaviour stimulates the DBO model, including the benefits of a stronger optimizer and faster convergence speed.

(1) Behavior of Ball rolling: Once there is no problem in the presence of the DB, it would utilize the sun for navigating after rolling dung balls. The location update equation for the DB's ball rolling is presented in Equation (9):

$$p_i(t+1) = p_i(t) + a \times k \times p_i(t-1) + b \times \Delta p \quad (9)$$

$$\Delta p = |p_i(t) - P^w|$$

Whereas t signifies the present iteration counts; $p_i(t)$ characterizes the location of the i th DB afterwards t th iterations; a represents the natural coefficient (there is deviation after $a = 1$). However, there is distraction from the new direction after $a = -1$), k refers to defecting coefficient, which contains constant values of $b \in (0,1)$; Δx mimics the changes in light intensity and P^w Represents a globally poor location.

(2) Behavior of dancing: Once the DB meets a problem and is prohibited from travel, it dances to relocate itself, and that is signified as Equation (10).

$$p_i(t+1) = p_i(t) + \tan(\theta) |p_i(t) - p_i(t+1)| \quad (10)$$

Here, θ characterizes the defection angle that captures the value $[0, \pi]$.

(3) Behavior of reproduction: DBS choose appropriate spawning places to offer safer surroundings for their offspring. Equation (11) reveals the region boundary selection approach to simulating DB spawn.

$$Lb^* = \max(P^* \times (1 - R), Lb)$$

$$Ub^* = \min(P^* \times (1 + R), Ub) \quad (11)$$

Now, Lb^* and Ub^* Epitomize the lower and upper boundaries of the spawn area individually and P^* signifies the present local optimum location. $R = \frac{1-t}{T_{\max}}$, T_{\max} signifies the set maximal iteration counts and Lb and Ub represent the upper and lower boundaries of the optimizer tackles. As the iteration counts improve, the spawn area becomes more dynamic, as presented in Equation (12).

$$T_i(t+1) = P^* + k_1 \times (T_i(t) - Lb^*) + k_2 \times (T_i(t) - Ub^*) \quad (12)$$

$T_i(t)$ represents the location of the i th DB egg at iteration t ; k_1 and k_2 signify randomly formed vectors of dimensions $1 \times D$, and D signifies the size of the optimizer difficulties.

(4) Behavior of Foraging: Developed DBs will excavate from the ground to search for food. Thus, they shall control the optimum region. The limitations of the optimum region are described as exposed in Equation (13).

$$Lb^b = \max(P^b \times (1 - R), Lb)$$

$$Ub^b = \min(P^b \times (1 + R), Ub) \quad (13)$$

Now, P^b characterizes the globally optimum foraging location, and Lb^b and Ub^b Symbolize the upper and lower limits of the optimum foraging region, correspondingly. The location of a more minor DB is upgraded, as exposed in Equation (14).

$$p_i(t + 1) = p_i(t) + k_3 \times (p_i(t) - Lb^b) + k_4 \times (p_i(t) - Ub^b) \quad (14)$$

Now, k_3 and k_4 characterize dual independent randomly generated numbers through the previous normal distributions and the later capturing values between (0-1).

(5) Behavior of stealing: DBs snip dung balls from others, characterized as Equation (15).

$$p_i(t + 1) = P^b + S \times g \times (|p_i(t) - P^*|) + (|p_i(t) - P^b|) \quad (15)$$

Now, S means constant, and g signifies randomly generated vectors of dimension $1 \times D$ and emulates normal distributions.

As the iteration counts improve, the DBO model accepts a lower convergence precision and executes local optimization. To deal with the limitations mentioned above, this paper performs a transverse and longitudinal crossover approach to decide the novel location of an objective after all updates utilizing the DBO model.

The longitudinal crossover model carries out vertical or horizontal crossovers in all generations in the iteration procedure, providing particular population sizes stuck in dimensioned local goals and possibilities to leap out of the iteration. Horizontal crossover is arithmetical amongst dual dissimilar individual particles of equal size within the population; the equation is as shown:

$$XS_{hc}(i, d) = r_1 * x(i, d) + (1 - r_1) * x(j, d) + c_1 * (x(i, d) - x(j, d)) \quad (16)$$

$$XS_{hc}(j, d) = r_1 * x(j, d) + (1 - r_1) * x(i, d) + c_2 * (x(j, d) - x(i, d)) \quad (17)$$

Here, $x(i, d)$ and $x(j, d)$ epitomize the d th size of the individual particles $x(i)$ and $x(j)$ in the parent population, individually; $XS_{hc}(i, d)$ and $XS_{hc}(j, d)$ symbolize the d th size child of $x(i, d)$ and $x(j, d)$ produced by subsequent crossover, individually; r_1 and r_2 signify [0,1] randomly generated numbers; and c_1 and c_2 characterize [1, 1] a randomly generated number.

The achieved offspring are compared with the parents to maintain the individuals by smaller target functions. The lower and upper choices of equal size are identical for dissimilar individual particles. c_1 and c_2 represent learning features. Therefore, the third term might improve the search range and discover the finest at the edge.

Longitudinal crossover is arithmetical amongst dual diverse sizes of the particles inside the population, while some samples per individual upgrade just for the sizes,

leaving the other sizes unchanged. That is represented through the succeeding equation:

$$XS_{lc}(i, d_1) = r * x(i, d_1) + (1 - r) * x(i, d_2) \quad (18)$$

Here $x(i, d_1)$ and $x(i, d_2)$ represent the d_1 and d_2 individual particle's dimensions $x(i)$, $XS(i, d)$ embodies the d_1 dimensioned offspring of the d_1 and d_2 sizes of $x(i)$ generated by longitudinal crossover. The resultant offspring are associated with their parents for maintaining the individuals by reduced target functions.

Fitness selection is the major factor that affects the accomplishment of the IDBO model. The hyperparameter selection comprises the solution encoder technique to assess the candidate outputs. The IDBO model considers precision as the key measure to project the fitness function, which is shown in Equation (19).

$$Fitness = \max(P) \quad (19)$$

Here, TP epitomizes the true positive, and FP indicates the false positive value.

4. Performance Validation

The RFIADRD-IDBODTLT method is investigated under the DR detection dataset [30]. Table 1 describes the dataset. Figure 3 depicts the sample images.

Table 1. Details of the dataset

Scale	DR	Images
0	No DR	5000
1	Mild	2000
2	Moderate	5000
3	Severe	800
4	Proliferative DR	700
Total		13500

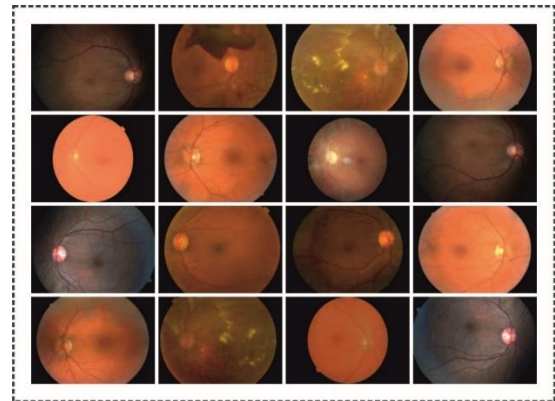


Fig. 3 Sample images

Figure 4 signifies the classifier results of the RFIADRD-IDBODTLT method under 80:20 of TRASE/TESSSE. The

confusion matrices exhibit precise classification and detection of all four classes, as shown in Figure 4(a)-4(b). The PR study, which illustrated superior output over four classes, is depicted in Figure 4(c). Eventually, the ROC study, which demonstrates skilful performances through great ROC values for four dissimilar classes, is represented in Figure 4(d).

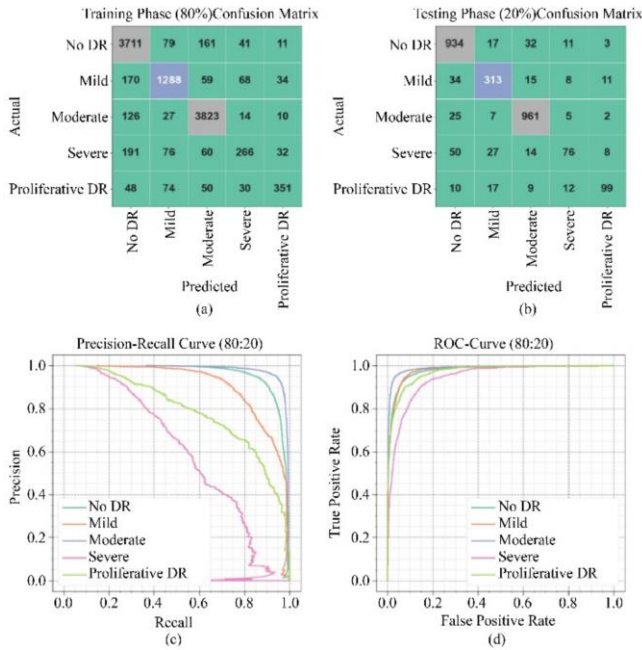


Fig. 4 80:20 of TRASE/TESE (a-b) confusion matrices and (c-d) PR and ROC curves

Table 2. DR detection output of RFIADRD-IBDODTLT method under 80:20 of TRASE/TESE

Classes	$Accu_y$	$Prec_n$	$Sens_y$	$Spec_y$	$F1_{score}$
TRASE (80%)					
No DR	92.34	87.40	92.71	92.13	89.97
Mild	94.56	83.42	79.56	97.21	81.44
Moderate	95.31	92.05	95.57	95.15	93.78
Severe	95.26	63.48	42.56	98.50	50.96
Proliferative DR	97.32	80.14	63.47	99.15	70.84
Average	94.96	81.30	74.77	96.43	77.40
TESSE (20%)					
No DR	93.26	88.70	93.68	93.01	91.12
Mild	94.96	82.15	82.15	97.07	82.15
Moderate	95.96	93.21	96.10	95.88	94.63
Severe	95.00	67.86	43.43	98.57	52.96
Proliferative DR	97.33	80.49	67.35	99.06	73.33
Average	95.30	82.48	76.54	96.72	78.84

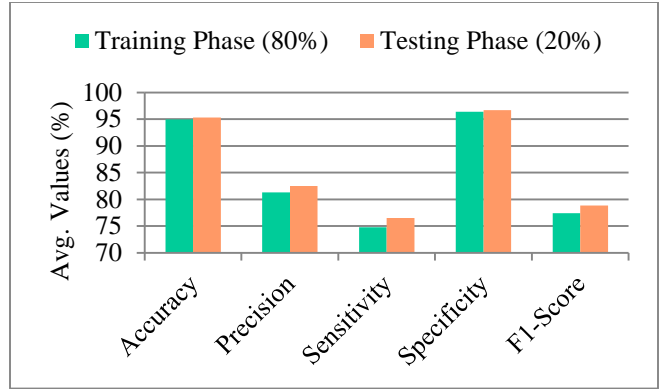


Fig. 5 Average of RFIADRD-IBDODTLT method under 80:20 of TRASE/TESE

Table 2 and Figure 5 depict an overall DR detection solution of the RFIADRD-IBDODTLT technique under 80:20 of TRASE/TESE. The performances exemplify that the RFIADRD-IBDODTLT technique is appropriately renowned for varied classes. On 80%TRASE, the RFIADRD-IBDODTLT technique presents an average $accu_y$, $prec_n$, $sens_y$, $spec_y$, and $F1_{score}$ of 94.96%, 81.30%, 74.77%, 96.43%, and 77.40%, correspondingly. In addition, with 20%TESSE, the RFIADRD-IBDODTLT model presents an average $accu_y$, $prec_n$, $sens_y$, $spec_y$, and $F1_{score}$ of 95.30%, 82.48%, 76.54%, 96.72%, and 78.84%, respectively.

Figure 6 depicts the TRA $accu_y$ (TRACY) and validation $accu_y$ (VLAAY) results of the RFIADRD-IBDODTLT method under 80:20 of TRASE/TESE. The $accu_y$ Value is computed in a period of 0-25 epochs. The figure illustrated that the TRACY/VLAAY values increased, showing the proficiency of the RFIADRD-IBDODTLT approach with lesser performance through multiple epochs. Moreover, the TRACY/VLAAY values increase over epochs, depicting lesser overfitting and higher performance of the RFIADRD-IBDODTLT approach, guaranteeing increased computation on hidden samples.

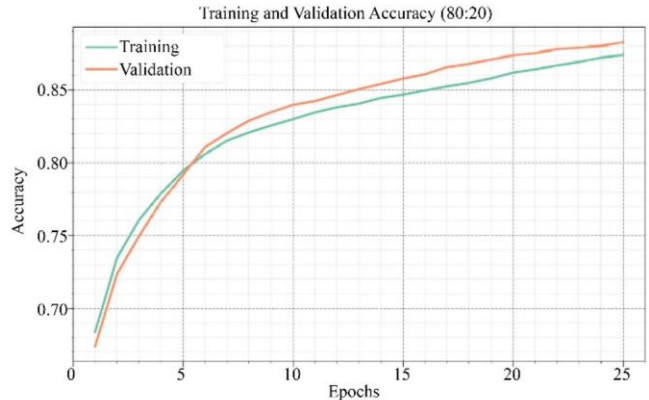


Fig. 6 $Accu_y$ curve of RFIADRD-IBDODTLT method under 80:20 of TRASE/TESE

Figure 7 depicts the TRA loss (TRALO) and VLA loss (VLALO) graph of the RFIADRD-IDBODTLT method under 80:20 of TRASE/TESSE. The loss is calculated across a period of 0-25 epochs. The TRALO/VLALO values demonstrate a lesser trend, indicating the RFIADRD-IDBODTLT model's capacity to harmonize a tradeoff among generalization data fitting. The steady decline in loss and accuracy values reflects the RFIADRD-IDBODTLT model's optimal performance, with results progressively refined.

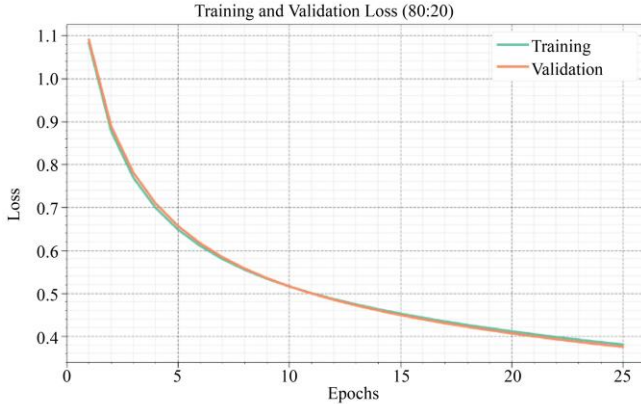


Fig. 7 Loss curve of RFIADRD-IDBODTLT method under 80:20 of TRASE/TESSE

Figure 8 depicts the classifier outputs of the RFIADRD-IDBODTLT methodology on 70:30 of TRASE/TESSE. Figure 8(a)-8(b) indicates the confusion matrix showing precise classification and detection of all four distinct classes. Figure 8(c) illustrates the PR study, which illustrated enhanced performance over 4 classes. Finally, Figure 8(d) signifies the ROC study, which showcases capable performances with higher ROC values for four classes.

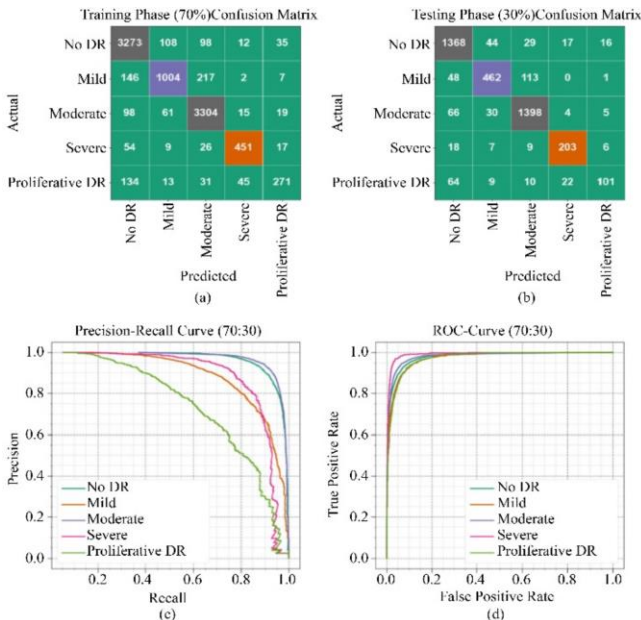


Fig. 8 70:30 of TRASE/TESSE (a-b) confusion matrix, and (c-d) PR and ROC curves.

Table 3 and Figure 9 illustrate the global DR detection results of the RFIADRD-IDBODTLT approach below 70:30 of TRASE/TESSE. The performances signify that the RFIADRD-IDBODTLT technique is accurately renowned for dissimilar classes. On 70%TRASE, the RFIADRD-IDBODTLT technique provides an average $accu_y$, $prec_n$, $sens_y$, $spec_y$, and $F1_{score}$ of 95.14%, 85.16%, 79.22%, 96.48%, and 81.68%, respectively. Additionally, on 30% TESSE, the RFIADRD-IDBODTLT technique provides an average $accu_y$, $prec_n$, $sens_y$, $spec_y$, and $F1_{score}$ of 94.88%, 84.33%, 78.49%, 96.32%, and 80.65%, subsequently.

Table 3. DR detection of RFIADRD-IDBODTLT technique under 70:30 of TRASE/TESSE

Classes	$Accu_y$	$Prec_n$	$Sens_y$	$Spec_y$	$F1_{score}$
TRASE (70%)					
No DR	92.75	88.34	92.82	92.71	90.53
Mild	94.04	84.02	72.97	97.63	78.10
Moderate	94.02	89.88	94.48	93.75	92.12
Severe	98.10	85.90	80.97	99.17	83.36
Proliferative DR	96.81	77.65	54.86	99.13	64.29
Average	95.14	85.16	79.22	96.48	81.68
TESSE (30%)					
No DR	92.54	87.47	92.81	92.39	90.06
Mild	93.78	83.70	74.04	97.37	78.57
Moderate	93.43	89.67	93.01	93.68	91.31
Severe	97.95	82.52	83.54	98.87	83.03
Proliferative DR	96.72	78.29	49.03	99.27	60.30
Average	94.88	84.33	78.49	96.32	80.65

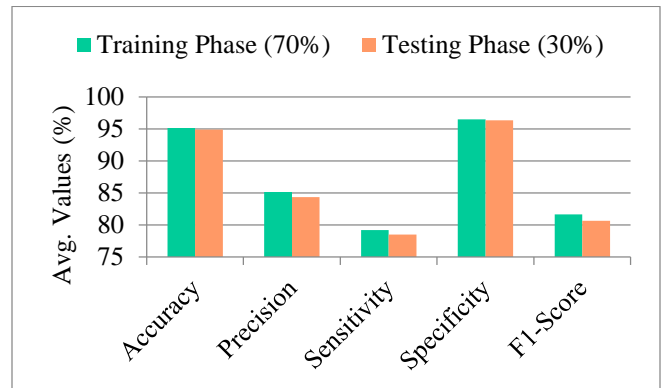


Fig. 9 Average of RFIADRD-IDBODTLT technique under 70:30 of TRASE/TESSE

Figure 10 depicts the TRAAAY/VLAAY results of the RFIADRD-IDBODTLT technique below 70:30 of TRASE/TESSE over a period of 0-25 epochs, which

illustrated that the TRAA_y/VLA_y values increased, indicating the proficiency of the RFIADRD-IBDODTLT approach with higher performance across diverse epochs. Moreover, the close TRAA_y/VLA_y values across epochs depict minimal overfitting and emphasize the robust performance and reliable predictions of the RFIADRD-IBDODTLT approach on unseen data.

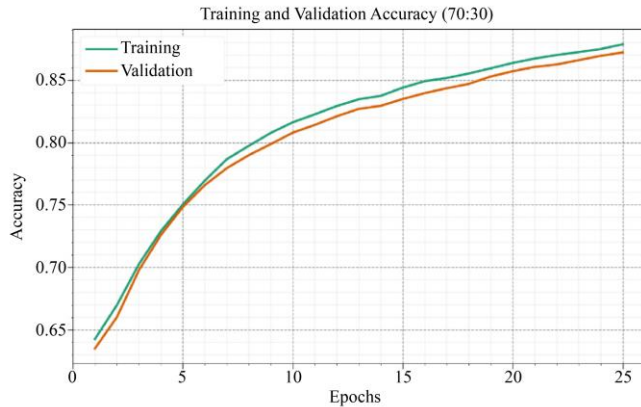


Fig. 10 *Accu_y* curve of RFIADRD-IBDODTLT model under 70:30 of TRASE/TESSE

Figure 11 depicts the TRALO/VLALO graph of the RFIADRD-IBDODTLT approach below 70:30 of TRASE/TESSE across 0-25 epochs. The TRALO/VLALO values indicate the RFIADRD-IBDODTLT approach effectively balances data fitting and generalization, with a consistent decrease in loss values reflecting its robust predictive performance.

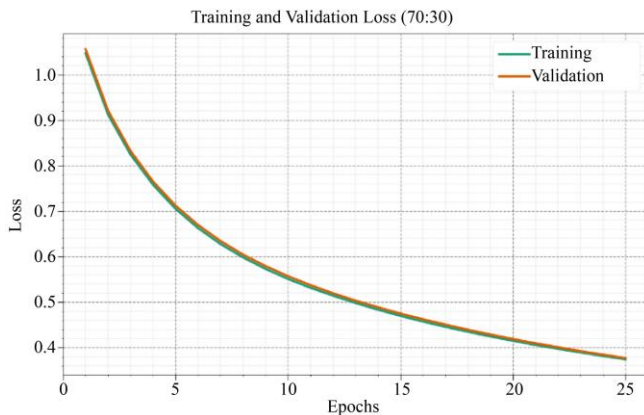


Fig. 11 Loss curve of RFIADRD-IBDODTLT technique under 70:30 of TRASE/TESSE

In Table 4 and Figure 12, the comparison analysis of the RFIADRD-IBDODTLT method with existing models is presented [31, 32]. The performances imply that the DI-AFIPADRG, CoT-Xnet, and DeepMT-DR techniques exhibited lesser values of *accu_y* and *F1_{score}*. Simultaneously, the STMF-DRNet, STMF-Net, and CABNet-IDRG techniques have reached marginally higher

accu_y and *F1_{score}*. Likewise, the ADAGDR-RIIAC and ADDR-SMBC techniques showed closer values of *accu_y* and *F1_{score}*. Additionally, the RFIADRD-IBDODTLT model results in improved *accu_y* and *F1_{score}* Of 95.30% and 78.84%, respectively.

Table 4. Comparison analysis of the RFIADRD-IBDODTLT methodology with existing methods [31, 32]

Method	<i>Accu_y</i>	<i>Sens_y</i>	<i>Spec_y</i>	<i>F1_{score}</i>
DeepMT-DR	85.70	70.31	80.42	75.31
CoT-Xnet	84.10	71.65	84.03	76.59
STMF-DRNet	86.30	74.30	81.08	73.09
STMF-Net	86.30	72.74	87.67	72.61
ADDR-SMBC	93.44	72.89	75.91	72.31
ADAGDR-RIIAC	92.23	72.65	78.56	75.49
DI-AFIPADRG	83.70	72.32	85.26	76.76
CABNet-IDRG	86.18	75.48	87.53	70.19
RFIADRD-IBDODTLT	95.30	76.54	96.72	78.84

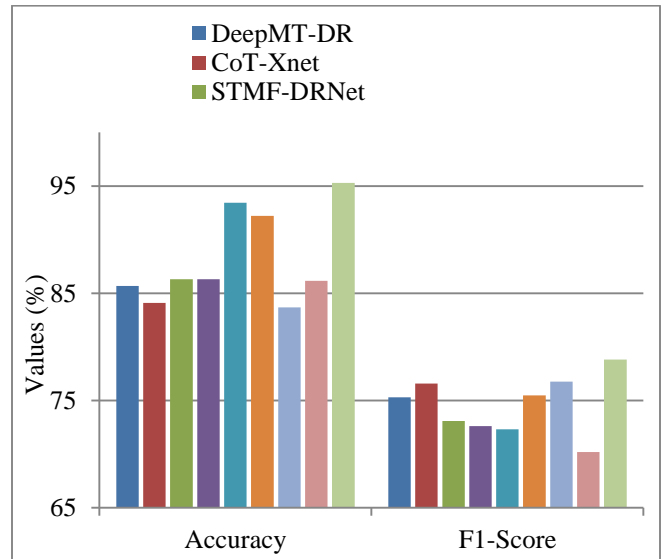


Fig. 12 *Accu_y* and *F1_{score}* of RFIADRD-IBDODTLT methodology with existing methods

Figure 13 presents a comparative *sens_y* and *spec_y* Results of the RFIADRD-IBDODTLT approach. The performances suggest that the DI-AFIPADRG, CoT-Xnet, and DeepMT-DR approaches have exemplified poorer values of *sens_y* and *spec_y*. Afterwards, the STMF-DRNet, STMF-Net, and CABNet-IDRG approaches have gained moderately enhanced *sens_y* and *spec_y*. Likewise, the ADAGDR-RIIAC and ADDR-SMBC approaches have revealed closer values of *sens_y* and *spec_y*. However, the RFIADRD-IBDODTLT model results in maximum performance with *sens_y* and *spec_y* Of 76.54% and 96.72%, respectively.

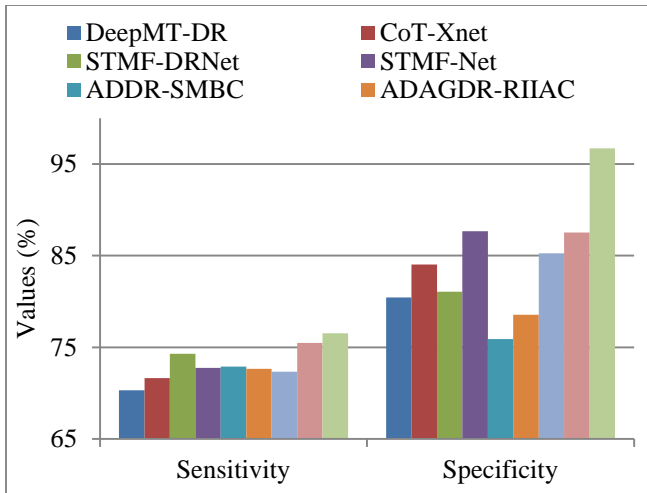


Fig. 13 Sens_y and spec_x of RFIADRD-IBBODTLT methodology with existing methods

5. Conclusion

In this study, an RFIADRD-IBBODTLT method is presented. The introduced RFIADRD-IBBODTLT approach relies on the advanced and automatic model for DR classification and grading on fundus images. The proposed RFIADRD-IBBODTLT model applies an image pre-processing stage using SF to remove noise in an input image dataset to accomplish this. Also, the CapsNet model is employed for feature extraction. For the DR classification, the BiLSTM approach is implemented. Finally, the hyperparameter selection of the BiLSTM model is performed by executing the Improved Dung Beetle Optimization (IDBO) model. Experimentation is performed to validate the RFIADRD-IBBODTLT approach under the DR detection dataset. The performance validation of the RFIADRD-IBBODTLT approach demonstrated a superior accuracy value of 95.30% over existing models.

References

- [1] Wejdan L. Alyoubi, Wafaa M. Shalash, and Maysoon F. Abulkhair, "Diabetic Retinopathy Detection through Deep Learning Techniques: A Review," *Informatics in Medicine Unlocked*, vol. 20, pp. 1-11, 2020. [[CrossRef](#)] [[Google Scholar](#)] [[Publisher Link](#)]
- [2] Early Treatment Diabetic Retinopathy Study Research Group, "Grading Diabetic Retinopathy from Stereoscopic Color Fundus Photographs-An Extension of the Modified Airlie House Classification: ETDRS Report Number 10," *Ophthalmology*, vol. 127, no. 4, pp. S99-S119, 2020. [[CrossRef](#)] [[Google Scholar](#)] [[Publisher Link](#)]
- [3] Md Mohaimenul Islam et al., "Deep Learning Algorithms for Detection of Diabetic Retinopathy in Retinal Fundus Photographs: A Systematic Review and Meta-Analysis," *Computer Methods and Programs in Biomedicine*, vol. 191, 2020. [[CrossRef](#)] [[Google Scholar](#)] [[Publisher Link](#)]
- [4] Prawej Ansari et al., "Diabetic Retinopathy: An Overview on Mechanisms, Pathophysiology and Pharmacotherapy," *Diabetology*, vol. 3, no. 1, pp. 159-175, 2022. [[CrossRef](#)] [[Google Scholar](#)] [[Publisher Link](#)]
- [5] Andrzej Grzybowski et al., "Artificial Intelligence for Diabetic Retinopathy Screening Using Color Retinal Photographs: From Development to Deployment," *Ophthalmology and Therapy*, vol. 12, pp. 1419-1437, 2023. [[CrossRef](#)] [[Google Scholar](#)] [[Publisher Link](#)]
- [6] Ling Dai et al., "A Deep Learning System for Detecting Diabetic Retinopathy across the Disease Spectrum," *Nature Communications*, vol. 12, no. 1, pp. 1-11, 2021. [[CrossRef](#)] [[Google Scholar](#)] [[Publisher Link](#)]
- [7] Zhixi Li et al., "An Automated Grading System for Detection of Vision-Threatening Referable Diabetic Retinopathy on the Basis of Color Fundus Photographs," *Diabetes Care*, vol. 41, no. 12, pp. 2509-2516, 2018. [[CrossRef](#)] [[Google Scholar](#)] [[Publisher Link](#)]
- [8] Sajib Kumar Saha et al., "Color Fundus Image Registration Techniques and Applications for Automated Analysis of Diabetic Retinopathy Progression: A Review," *Biomedical Signal Processing and Control*, vol. 47, pp. 288-302, 2019. [[CrossRef](#)] [[Google Scholar](#)] [[Publisher Link](#)]
- [9] Avnish Panwar et al., *Stratification of the Lesions in Color Fundus Images of Diabetic Retinopathy Patients Using Deep Learning Models and Machine Learning Classifiers*, Edge Analytics, Springer, Singapore, pp. 653-666, 2022. [[CrossRef](#)] [[Google Scholar](#)] [[Publisher Link](#)]
- [10] Zainab Sami Yaseen, "Using Major Pathway and Compound Analysis Methods to Identify Factors Affecting Diabetes," *Pure Mathematics for Theoretical Computer Science*, vol. 3, no. 1, pp. 31-47, 2024. [[CrossRef](#)] [[Google Scholar](#)] [[Publisher Link](#)]
- [11] Lavanya Ravala, and G.K. Rajini, "Optimized Deep Learning Based Approach for Enhanced frame Work of Automated Diagnosis of Diabetic Retinopathy," *Research Journal of Pharmacy and Technology*, vol. 17, no. 9, pp. 4443-4448, 2024. [[CrossRef](#)] [[Google Scholar](#)] [[Publisher Link](#)]
- [12] Pradeep Kumar Jena et al., "A Novel Approach for Diabetic Retinopathy Screening Using Asymmetric Deep Learning Features," *Big Data and Cognitive Computing*, vol. 7, no. 1, pp. 1-16, 2023. [[CrossRef](#)] [[Google Scholar](#)] [[Publisher Link](#)]
- [13] G. Sivapriya et al., "Automated Diagnostic Classification of Diabetic Retinopathy with Microvascular Structure of Fundus Images Using Deep Learning Method," *Biomedical Signal Processing and Control*, vol. 88, 2024. [[CrossRef](#)] [[Google Scholar](#)] [[Publisher Link](#)]
- [14] Thangam Palaniswamy, and Mahendiran Vellingiri, "Internet of Things and Deep Learning Enabled Diabetic Retinopathy Diagnosis Using Retinal Fundus Images," *IEEE Access*, vol. 11, pp. 27590-27601, 2023. [[CrossRef](#)] [[Google Scholar](#)] [[Publisher Link](#)]
- [15] Lakshay Arora et al., "Ensemble Deep Learning and Efficientnet for Accurate Diagnosis of Diabetic Retinopathy," *Scientific Reports*, vol. 14, no. 1, pp. 1-16, 2024. [[CrossRef](#)] [[Google Scholar](#)] [[Publisher Link](#)]

- [16] Zhijiang Wan et al., “A Wireless Sensor System for Diabetic Retinopathy Grading Using MobileViT-Plus and ResNet-Based Hybrid Deep Learning Framework,” *Applied Sciences*, vol. 13, no. 11, pp. 1-18, 2023. [[CrossRef](#)] [[Google Scholar](#)] [[Publisher Link](#)]
- [17] F.M. Javed Mehedi Shamrat et al., “An Advanced Deep Neural Network for Fundus Image Analysis and Enhancing Diabetic Retinopathy Detection,” *Healthcare Analytics*, vol. 5, pp. 1-19, 2024. [[CrossRef](#)] [[Google Scholar](#)] [[Publisher Link](#)]
- [18] Nouf Al-Kahtani et al., “Discrete Migratory Bird Optimizer with Deep Transfer Learning Aided Multi-Retinal Disease Detection on Fundus Imaging,” *Results in Engineering*, vol. 26, pp. 1-14, 2025. [[CrossRef](#)] [[Google Scholar](#)] [[Publisher Link](#)]
- [19] Asif Raza et al., “Enhancing Medical Image Classification through PSO-Optimized Dual Deterministic Approach and Robust Transfer Learning,” *IEEE Access*, vol. 12, pp. 177144-177159, 2024. [[CrossRef](#)] [[Google Scholar](#)] [[Publisher Link](#)]
- [20] A.M. Mutawa et al., “Randomization-Driven Hybrid Deep Learning for Diabetic Retinopathy Detection,” *IEEE Access*, vol. 13, pp. 38901-38913, 2025. [[CrossRef](#)] [[Google Scholar](#)] [[Publisher Link](#)]
- [21] Krishnamoorthy Natarajan et al., “A Novel Method for the Detection and Classification of Multiple Diseases Using Transfer Learning-Based Deep Learning Techniques with Improved Performance,” *Neural Computing and Applications*, vol. 36, pp. 18979-18997, 2024. [[CrossRef](#)] [[Google Scholar](#)] [[Publisher Link](#)]
- [22] Mishmala Sushith et al., “A Hybrid Deep Learning Framework for Early Detection of Diabetic Retinopathy Using Retinal Fundus Images,” *Scientific Reports*, vol. 15, no. 1, pp. 1-31, 2025. [[CrossRef](#)] [[Google Scholar](#)] [[Publisher Link](#)]
- [23] Sundreen Asad Kamal et al., “DRSegNet: A Cutting-Edge Approach to Diabetic Retinopathy Segmentation and Classification Using Parameter-Aware Nature-Inspired Optimization,” *PloS One*, vol. 19, no. 12, pp. 1-40, 2024. [[CrossRef](#)] [[Google Scholar](#)] [[Publisher Link](#)]
- [24] Ravi Bhushan Dixit, and Chandan Kumar Jha, “Fundus Image Based Diabetic Retinopathy Detection Using EfficientNetB3 with Squeeze and Excitation Block,” *Medical Engineering & Physics*, vol. 140, 2025. [[CrossRef](#)] [[Google Scholar](#)] [[Publisher Link](#)]
- [25] Telagarapu Prabhakar et al., “Exponential Gannet Firefly Optimization Algorithm Enabled Deep Learning for Diabetic Retinopathy Detection,” *Biomedical Signal Processing and Control*, vol. 87, 2024. [[CrossRef](#)] [[Google Scholar](#)] [[Publisher Link](#)]
- [26] Danial Sharifrazi et al., “Fusion of Convolution Neural Network, Support Vector Machine and Sobel Filter for Accurate Detection of COVID-19 Patients Using X-Ray Images,” *Biomedical Signal Processing and Control*, vol. 68, pp. 1-14, 2021. [[CrossRef](#)] [[Google Scholar](#)] [[Publisher Link](#)]
- [27] Gunjan Shandilya et al., “Autonomous Detection of Nail Disorders Using a Hybrid Capsule CNN: A Novel Deep Learning Approach for Early Diagnosis,” *BMC Medical Informatics and Decision Making*, vol. 24, pp. 1-19, 2024. [[CrossRef](#)] [[Google Scholar](#)] [[Publisher Link](#)]
- [28] Khosro Rezaee et al., “Hand Gestures Classification of sEMG Signals Based on BiLSTM-Metaheuristic Optimization and Hybrid U-Net-MobileNetV2 Encoder Architecture,” *Scientific Reports*, vol. 14, no. 1, pp. 1-20, 2024. [[CrossRef](#)] [[Google Scholar](#)] [[Publisher Link](#)]
- [29] Yinglei Li et al., “Research on Optimization of Target Positioning Error Based on Unmanned Aerial Vehicle Platform,” *Applied Sciences*, vol. 14, no. 24, pp. 1-18, 2024. [[CrossRef](#)] [[Google Scholar](#)] [[Publisher Link](#)]
- [30] Will Cukierski, Diabetic Retinopathy Detection, Kaggle. [Online]. Available: <https://www.kaggle.com/c/diabetic-retinopathy-detection/>
- [31] Yuanyuan Liu et al., “STMF-DRNet: A Multi-Branch Fine-Grained Classification Model for Diabetic Retinopathy Using Swin-TransformerV2,” *Biomedical Signal Processing and Control*, vol. 103, pp. 1-12, 2025. [[CrossRef](#)] [[Google Scholar](#)] [[Publisher Link](#)]
- [32] Yanxia Liu, “Automatic Grading Diabetic Retinopathy in Color Fundus Image: Cascaded Hybrid Attention Network,” *Journal of Radiation Research and Applied Sciences*, vol. 17, no. 4, pp. 1-5, 2024. [[CrossRef](#)] [[Google Scholar](#)] [[Publisher Link](#)]
- [33] Roberto Romero-Oraá et al., “Attention-Based Deep Learning Framework for Automatic Fundus Image Processing to Aid in Diabetic Retinopathy Grading,” *Computer Methods and Programs in Biomedicine*, vol. 249, pp. 1-10, 2024. [[CrossRef](#)] [[Google Scholar](#)] [[Publisher Link](#)]